

## Article

# Assessment of Defects under Insulation Using K-Medoids Clustering Algorithm-Based Microwave Nondestructive Testing

Shin Yee Tan <sup>1</sup>, Muhammad Firdaus Akbar <sup>1,\*</sup> , Nawaf H. M. M. Shrifan <sup>2</sup> , Ghassan Nihad Jawad <sup>3</sup>  
and Mohd Nadhir Ab Wahab <sup>4,\*</sup> 

<sup>1</sup> School of Electrical and Electronic Engineering, Universiti Sains Malaysia, Nibong Tebal 14300, Penang, Malaysia

<sup>2</sup> Faculty of Oil and Minerals, University of Aden, Shabwah, Yemen

<sup>3</sup> Department of Electronics and Communication Engineering, University of Baghdad, Baghdad 10071, Iraq

<sup>4</sup> School of Computer Sciences, Universiti Sains Malaysia, Gelugor 11800, Penang, Malaysia

\* Correspondence: firdaus.akbar@usm.my (M.F.A.); mohdnadhir@usm.my (M.N.A.W.)

**Abstract:** Composite insulations, such as ceramics, are commonly utilized in the turbine system as a thermal coating barrier to protect the metal substrate against high temperatures and pressure. The presence of delamination in the composite insulations may cause turbine failure, leading to a catastrophic accident. Thus, regular non-destructive testing is required to detect and evaluate insulation defects. Among the non-destructive testing techniques, the microwave technique has emerged as a promising method for assessing defects in ceramic coatings. Although the method is promising, microwave non-destructive testing suffers from poor spatial imaging, making the defect assessment challenging. In this paper, a novel technique based on microwave non-destructive testing with a k-medoids clustering algorithm for delamination detection is proposed. The representative ceramic coating sample is scanned using a Q-band open-ended rectangular waveguide with 101 frequency points that operated between 33 to 50 GHz. The measured data is transformed from the frequency domain to the time domain using an inverse fast Fourier transform. The principal component analysis is then used to reduce the dimensionality of 101 time steps into only 3 dominant attributes. The attributes of each inspected location are classified as defect or defect-free using the k-medoids clustering algorithm for accurately detecting and sizing the defects in the ceramic insulation. The results reported in this paper highlight the superiority of the k-medoids clustering algorithm in delamination detection, with an accuracy rate of 95.4%. This is a significant step forward compared to earlier approaches for identifying ceramic defects.

**Keywords:** ceramic insulation; defects under insulation; delamination; microwave non-destructive testing; clustering algorithm



**Citation:** Tan, S.Y.; Akbar, M.F.; Shrifan, N.H.M.M.; Nihad Jawad, G.; Ab Wahab, M.N. Assessment of Defects under Insulation Using K-Medoids Clustering Algorithm-Based Microwave Nondestructive Testing. *Coatings* **2022**, *12*, 1440. <https://doi.org/10.3390/coatings12101440>

Academic Editors: Youn ho Cho, Vimalathithan Paramasamy Kannan, Claudia Barile and Young H. Kim

Received: 14 August 2022

Accepted: 19 September 2022

Published: 30 September 2022

**Publisher's Note:** MDPI stays neutral with regard to jurisdictional claims in published maps and institutional affiliations.



**Copyright:** © 2022 by the authors. Licensee MDPI, Basel, Switzerland. This article is an open access article distributed under the terms and conditions of the Creative Commons Attribution (CC BY) license (<https://creativecommons.org/licenses/by/4.0/>).

## 1. Introduction

Metal substrates are often protected against corrosion and higher temperatures by a ceramic-based coating [1]. Ceramic coating is often used on the turbine blades, vanes, and combustors of gas turbines to improve thermal protection against steam and higher temperatures [2]. Subsurface defects, such as debonding and delamination, reduce the ceramic's lifespan. The integrity of the entire structure may be at risk if these defects continue to develop undetected. Therefore, precise and timely non-destructive testing (NDT) is necessary to minimize maintenance costs, increase productivity, and enhance the entire system's safety and dependability.

The detection of defects under ceramic coatings is difficult using conventional NDT techniques, including eddy current, thermography, and ultrasonic approaches, owing to field penetration restrictions when evaluating dielectric materials [3,4]. Due to the absence of induced currents, the eddy currents inspection method cannot be used to examine lossless dielectric materials [5]. Ceramic coating has a significant porosity, which results

in the ultrasonic waves being dispersed and drastically attenuated, lowering the defect detection accuracy [6]. On the other hand, the thermography test of the ceramic coating is challenging due to the existence of stains, roughed regions, eroded parts, and over-thickness of the coating, along with restricted optical access, making the interpretation of the thermographic imaging sequences difficult [7]. The present inspection routine involves removing coating material to permit examination, employing a traditional methods, such as the ultrasonic approach, then reapplying the coating, which is both expensive and time-consuming [8]. As a consequence, an alternative method of assessing ceramic coating for underlying defects is required.

Microwave NDT is a relatively new development as a sustainable option for identifying and assessing the defects in ceramic coatings without the need for its removal. While ultrasonic testing relies on direct interaction with the specimen being examined, or coupling, microwave NDT can penetrate the ceramic coatings. Dielectric coatings, such as ceramics, allow microwave signals to pass through them, interacting with their internal structure, and they are subjected to variations associated with boundary contacts [9]. The internal structures of certain composites, ceramics, and concrete interfere with electromagnetic waves traveling at microwave frequencies [10].

Defects under coatings are detected using numerous microwave NDT techniques [8,11–16]. In the work in [17], a microwave ground-signal-ground (GSG) probe is used to evaluate the delamination in metal with thermal barrier coatings (TBCs). The study suggests that the microwave GSG probe is capable of indicating the existence of delamination and its extent. However, there is still some delamination adjacent to the sloping edges that cannot yet be discovered in the sample examined using this technique. The accuracy of delamination detection is enhanced by the work in [18]. A ridge waveguide is employed to enhance delamination detection in ceramic-coated metal samples. The research illustrates that it is possible to accurately forecast delamination depth and size, with a 7.87 and 5% error rate, respectively. However, owing to the limited bandwidth and dispersive state of the waveguide, the waveguide delamination imaging remains low-resolution. There is a significant improvement in the spatial resolution of the defects in the work in [19]. In order to detect ceramic coating delamination, an electromagnetic sensor incorporating metamaterials is utilized [19]. In this study, ceramic zirconia is coated on stainless steel, mimicking the TBCs. The findings demonstrate that the sensor can identify the defect areas at microwave frequency. From the areas detected, the characterization of the defects can be carried out. However, it is necessary to be able to detect the extremely slight delamination in order to increase the accuracy of the microwave sensor.

The open-ended rectangular waveguide (OERW) inspection method is one of the most prevalent for under-coating inspection of very minor delamination. The microwave signal from the probe is directed by the OERW to the sample under the coating. The changes in resonant frequency, as well as the magnitude and phase of the microwave reflection coefficient, are used to image the defects, which are acquired using a vector network analyzer (VNA). OERWs are extensively utilized for microwave NDT applications, including the measurement of dielectric materials' properties [20], the thickness measurement of dielectric slabs [21,22], and the determination of porosity levels in ceramics [2]. The application of the OERW approach to discover undercoating defects is also emphasized in [5]. Although OERW results are promising, they possess several shortcomings in identifying ceramic coating delamination. In the near field, an OERW's spatial resolution depends on the probe's size. OERW microwave NDT applications regarding ceramic coatings have exhibited challenges such as a lack of high-quality spatial images and an inaccurate prediction of the size of the defects in ceramics, particularly when the probe dimensions are substantially bigger than the defect dimensions. Furthermore, due to the porosity of the ceramic coating, it is difficult to trace the defect under ceramic coatings at the micrometer range. It is futile to use quantitative or particular frequency domain interpretation to identify the defect across a ceramic coating and a metal as a result of changes in the ceramic's porosity and microstructure during cyclic services [2]. The frequency-domain characteristics of reflected microwave signals are dramatically altered

due to the ceramic modifications, making it more challenging to identify small delamination. Table 1 summarize the microwave NDT techniques.

**Table 1.** Comparison of microwave NDT techniques.

Ref. No.	Technique	Concept of Use	Advantages	Disadvantages
[17]	Microwave GSG probe	Delamination evaluation in metal with TBCs coating	Able to detect delamination and sizes.	Unable to detect delamination next to the sloping edges.
[18]	Ridge waveguide	Delamination evaluation in ceramic-coated metal	Able to detect delamination depth and size. Lower error rate.	Low-resolution imaging.
[19]	Electromagnetic sensor with metamaterials	Delamination evaluation in stainless steel with ceramic zirconia coating	Able to detect and characterize defects. Higher spatial resolution of defects.	Unable to detect small delamination. Lower accuracy rate.
[5]	OERW	Delamination evaluation in ceramic-coated metal	Able to detect very small delamination.	Low spatial image quality. Larger defect size prediction than the actual defect.

Microwave NDT techniques outperform conventional NDT techniques in defect detection under ceramic coatings. However, the accuracy rate is still low, as the porosity of the ceramic coating affects the permittivity changes in the reflected coefficients. The emergence of a post-processing algorithm along with microwave NDT techniques improves the defect detection accuracy, classifying defect and defect-free areas.

Various methods are used to investigate the source of the defect. Time-domain reflectometry (TDR) with inverse discrete Fourier transform (IDFT) is described in [23]. TDR is a technique for detecting delamination that involves delivering a pulse into the material and monitoring the time at which the pulse's reflection arrives. The peak amplitude variation of the back metal is studied to highlight the variance between the defect and defect-free zones in the back metal peak. The fluctuation with the peak of the amplitude of the back metal is a good indicator of the delamination in the ceramic coating. However, different frequency components exhibit varying delays in propagating their signals, which has an impact on pulse propagation. The authors of [24] introduce the concept of correlation analysis, which is unaffected by the lag in time. This technique aims to evaluate the ability and precision of defect characterization. A low correlation between two reflection coefficient vectors, which includes phase and magnitude, indicates the defect areas. This approach is capable of distinguishing the types of defects, including delamination and cracks on the metal. However, even in locations where there is no defect, the phase ripples from the discontinuity effect from the sample's edge cause contradictory correlation values. Moreover, this method necessitates the use of a non-defective sample as a point of comparison. Principal component analysis (PCA) does not require any pre-existing data or knowledge. Three primary sources of the obtained signal are partitioned using PCA [15,23,25]. The ceramic surface, the ceramic interior layer, and the back metal are all referred to as partitioned sources. The outer surface and inner ceramic layers may, however, conceal information about the minor defect. This results in a lack of considerable separation between the features, resulting in fuzzy margins around the defects. In [26], the nonnegative matrix factorization (NMF) is first presented to reveal the faulty sections of adhered ceramic claddings. Defect and defect-free areas are arbitrarily partitioned, based on spatial frequency characteristics. NMF is a statistical technique for shrinking and reassembling datasets that are dependent on their original dimensions. However, owing to the paucity of results in specific periods, an appropriate choice of examination time spans is essential. Moreover, deficient spectral resolution causes NMF to perform poorly [27].

On the other hand, microwave NDT-based machine learning has been suggested to improve the defect detection accuracy to compensate for low spectral resolution. A support vector machine (SVM) is utilized to quantify and detect ceramic samples' porosity [28]. SVM

represents kernel machines, which are intended to identify the most appropriate approach, enhancing the accuracy of predictions by randomly searching for the best path [29]. The SVM works effectively in categorizing the degree of porosity of ceramic samples; the classification error rate is reduced to 7.14%. The categorization inaccuracy is caused by data noise. In addition, training samples for supervised machine learning algorithms are also challenging to obtain in NDT applications due to the limited resources available for data acquisition. PCA is used in conjunction with supervised machine learning to minimize the data's noise. A principal component analysis-artificial neural network (PCA-ANN) classifier-based V-band horn antenna is proposed to categorize the cracks in the ceramic tiles [30]. Extracting features using PCA decreases the complexity of data by representing it in a lower-dimensional space. C-scan is used to visualize the PCA-processed data. C-scan images of PCA are used to depict the faulty areas of the sample under test. PCA shows its superiority by attaining a crack detection accuracy of 73.33%. However, in a similar manner to the SVM approach, the training dataset and its volatility have a major influence on the findings. Furthermore, since the PCA feature is the outcome of data dimensional reduction, it is unable to anticipate the depth of the defects.

Recently, efforts to integrate microwave NDT with the k-means clustering algorithm have been used to improve the efficiency and reliability of the inspection system [15]. The unsupervised k-means clustering algorithm does not require training samples for clustering the defect and defect-free areas. The k-means-based OERW is proposed to detect delamination in the glass fiber reinforced polymer (GFRP) down to a depth of 1 mm [15]. The k-means algorithm classified the inspected locations' microwave reflection coefficients in the defect and defect-free regions, which are then spatially displayed to identify delamination location and size. Compared to supervised machine learning algorithms, the k-means clustering algorithm shows superior performance in partitioning the inspected locations into the defect and defect-free categories without the use of a training sample. Aside from that, the proposed k-means clustering algorithm is also good at sharply separating the edges of the delamination and delamination-free regions. However, the identified defect size is slightly larger than the actual size. Table 2 summarizes the evaluation of the post-processing algorithm.

The hybridization of the post-processing algorithm with microwave NDT techniques improves the defect detection accuracy in terms of location, size, and depth. In addition, the defect and defect-free zones are distinguished. However, the fact that the predicted defect is larger than the actual defect, the blur margin around the defects, and the method's inability to identify minor defects affects the accuracy of the inspected delamination.

A novel microwave NDT approach based on the k-medoids clustering algorithm for delamination inspection in the ceramic coating is proposed in this study. There is currently no documentation of the k-medoids clustering algorithm's defect assessment in the literature. The proposed technique is used to identify and measure the size and location of the defects. OERW is utilized to sweep 101 frequency points from 33 to 50 GHz across the ceramic sample. Time-domain signals are translated from the acquired frequency-domain signals, employing inverse fast Fourier transform (IFFT). PCA is then used to reduce the dimensionality from 101 time-steps into 3 PCA components. Thereafter, the k-medoids algorithm is employed simultaneously to categorize the 3 components of the inspected locations into delamination and delamination-free areas for imaging the underlying disorders. The study findings are noteworthy because the suggested approach gives an on-site faults diagnosis based on the microwave NDT inspection framework in ceramic substances and can be used for quality assurance in manufacturing, as well as portable inspection in the field.

**Table 2.** Comparison summary of the post-processing algorithm.

	Techniques	Concept of Use	Advantages	Disadvantages
[23]	TDR-IDFT	Delamination evaluation in ceramic-coated metal	Able to characterize defect and defect-free areas.	Delay in signal propagation.
[24]	Correlation analysis	Delamination evaluation in ceramic-coated metal	Able to distinguish types of defects. Lag in time does not affect the results of defect inspection.	Inconsistent correlation values caused by sample's edge. Requires non-defective sample as a point of comparison.
[25]	PCA	Delamination evaluation in ceramic-coated metal	Does not require pre-existing data.	Unable to predict minor defects. Blur margin around defects.
[26]	NMF	Defect evaluation in adhered ceramic claddings	Able to distinguish defect and defect-free areas.	Accuracy affected by spectral resolution.
[28]	SVM	Porosity detection in ceramics	Able to categorize degree of porosity of ceramics.	Categorization inaccuracy affected by data noise. Training samples are limited.
[30]	PCA-ANN	Crack categorization in ceramic tiles	Able to detect cracks.	Training samples are limited. Unable to anticipate the depth of the defect.
[15]	k-means	Delamination detection in GFRP	Does not require training samples. Able to sharply separate the edges of defect and defect-free areas. Able to identify delamination size.	Identified defect size is larger than actual defect size.

After presenting the introduction herein, Section 2 of this paper provides an overview of defect detection based on the microwave OERW probe and reflection coefficients in the time domain, followed by an introduction to the k-medoids clustering algorithm. Section 2.4 demonstrates the approach. The findings of the deliberations are presented in Section 3. Finally, Section 4 offers a general conclusion to the research.

## 2. Materials and Methods

### 2.1. Open-Ended Rectangular Waveguide (OERW)

The OERW operates at 33 to 50 GHz in the Q-band millimeter-wave frequency spectrum. This frequency range is selected to procure adequate wave penetration with high depth resolution [31]. The OERW is placed on a virtual reference plan to scan a metal-backed sample with a ceramic coating. The sample under test is positioned near the OERW at a standoff distance. Figure 1 presents the cross-section of OERW with inspection of a sample under test without delamination, showing a trellis diagram indicating the behavior of the incident wave and its multiple reflections. It is worth noting that the standoff distance shown in the figure is assumed to be a fraction of the shortest wavelength within the frequency range of operation. This condition is set to ensure that the electromagnetic wave distribution of the waveguide's open end is maintained at the sample's surface.

In Figure 1, the incident wave,  $t_0$  transmits from the OERW to the test sample. The wave is reflected as soon as it reaches the ceramic and metal surface, denoted as  $t_1$  and  $t_2$ , respectively. The time required for the microwave signal for be reflected from the sample under test is recorded. The  $t_1$  and  $t_2$  for the sample under test without delamination are taken as references. Figure 2 depicts the situation in the event of a delamination flaw.  $t'_1$ ,  $t'_2$ , and  $t'_3$  are the three waves that reflect from the sample under test to the OERW.

The incident waves take  $t'_1$ ,  $t'_2$ , and  $t'_3$  s to reflect off the ceramic surface, the delamination border, and the back metal, correspondingly. The time required for the  $t_2$  is different from the  $t'_2$ , where  $t_2 \neq t'_2$ . Thus, it is possible to deduce that the ceramic coating has delamination. Nevertheless, the arrival time of the reflection cannot be utilized to assess the size and the precise distance of the delamination from the sources. This is due to the assumption that the distance between the OERW probe and the sample under test is relatively minimal. The non-linear phenomena, including waveform dispersing and frequency sweeping, are mitigated to curtail in this near-field environment [15].

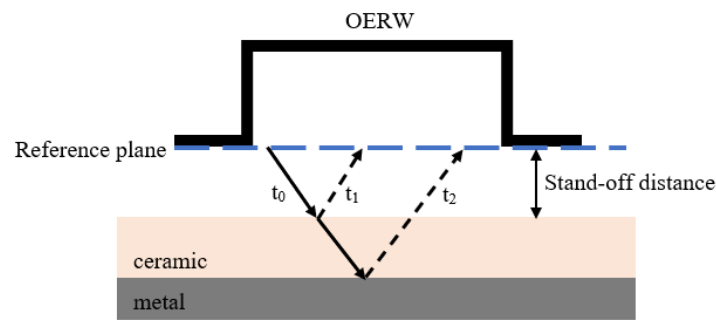


**Figure 1.** Cross-section of an OERW and the trellis diagram of the incident wave, with its multiple reflections, which are incident wave,  $t_0$ , reflected wave from ceramic and metal surface,  $t_1$  and  $t_2$ , respectively, of a sample under test without delamination.

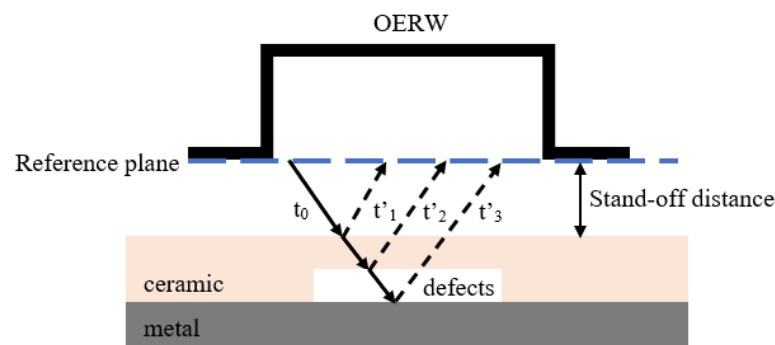


**Figure 2.** Cross-section of an OERW and the trellis diagram of the incident wave, with its multiple reflections, which are incident wave,  $t_0$ , reflected wave from ceramic, delamination border and metal surface,  $t'_1$ ,  $t'_2$  and  $t'_3$ , correspondingly, of a sample under test with delamination.

The OERW uses frequency sweeping to operate. A frequency sweeping is used to determine the bandwidth of a system, as well as to construct a transfer function [32]. The reflection coefficient obtained by the vector network analyzer (VNA) is subjected to IFFT. This is accomplished to acquire the discrete refractive index at the incident surface with respect to time. In the case of the defect-free region, the magnitude of  $t_1$  and  $t_2$  remain at their peak. On the other hand, when the  $t'_2$  magnitude is not at its peak, it can be classified as a defect zone. When compared to the magnitude of  $t_2$  obtained from the defect-free region, the magnitude of  $t'_2$ , which is meant to represent the second peak, decreases. As a result, any decrease in the magnitude of the second peak can infer that delamination occurs in the ceramic coating. The defect and defect-free zones can be simply grouped utilizing the magnitude of the reflected microwave signals in the time domain using this deduction [33].

Notably, determining the IFFT with a greater number of points offers a better representation of the reflecting pulse, since it performs oversampling in the time domain. There is a downside, however, as oversampling significantly increases the detection time and processing complexity [33]. Therefore, PCA is required to reduce dimensionality.

## 2.2. Principal Component Analysis (PCA)

PCA is offered as a method to reduce the large dimensions of space data to the dimensions of the smallest spaces [34]. It is considered as a multivariate analysis approach that seeks to keep the variance as feasible as possible while reducing repetition [35]. This is achieved by computing the eigenvalues and eigenvectors of the covariance matrix. Each PCA component is the result of a linear combining of the original responses. The eigenvectors or PCA components correspond to the maximum eigenvalues in the data relating to the dominant PCA component [36]. PCA maintains the original data of the

PCA components with maximum variances. In the following, (1) shows the calculation of eigenvectors and eigenvalues, while (2) is the equation of the covariance matrix [37].

$$C_x v_m = \lambda_m v_m \quad (1)$$

where  $m$  is the data dimension,  $C_x$  is the covariance matrix,  $v_m$  is the eigenvectors, and  $\lambda_m$  is the eigenvalues.

$$C_x = \frac{1}{n-1} \sum_{i=1}^n (X_i - \bar{X})(X_i - \bar{X})^T \quad (2)$$

where  $n$  is the number of observation data,  $X_i$  is the observation data at the  $i$  inspected location, and  $\bar{X}$  is the mean data. Figure 3 shows the process of dimensionality reduction using PCA.

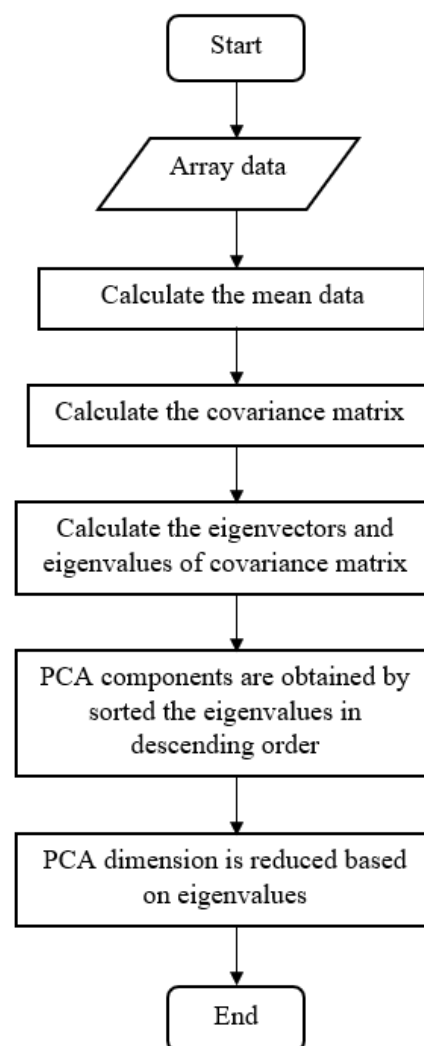


**Figure 3.** Process of dimensionality reduction using PCA.

The eigenvalue decomposition based on mean data maximizes the covariance matrix. Then, in the column and row-wise direction, two-directional projection matrices in the x- and y-direction are obtained [38]. Lower-order PCA components have a more significant degree of variance than higher-order PCA components, and the first PCA component explains the greatest variation [39]. As a consequence, if the response of the concealed delamination varies significantly, the hidden defect features will be highlighted in the low-order PCA components. The initial number of the PCA component could therefore be utilized to

reassemble the images, whereby hidden fracture characteristics can be highlighted. It has been shown that feature selection conducted using PCA as a preprocessing step is quite beneficial in decreasing computing time and increasing accuracy [40]. Moreover, it is possible to identify the clusters of samples with identical characteristics by visualizing the PCA components using a graph [41]. However, PCA exhibits a relatively high computational cost, as well as technical problems in the parallelizing algorithm [42].

### 2.3. K-Medoids Clustering Algorithm

The clustering method seeks to organize the observed collection of data into discrete groups. The k-medoids grouping method is among the unsupervised machine learning strategies used to handle sorting issues. K-medoids is also known as partitioning around medoids (PAM). Since each cluster is represented by one representative object, the primary idea behind the k-medoids clustering algorithm is to assign the other objects to the representative objects that are the most similar to the selected objects [43]. Since there is a representative for each cluster, instead of a cluster center, k-medoids are more resilient in terms of noise and outliers, compared to the k-means algorithm [44]. K-medoids attempt to significantly minimize the objective function  $J_m$ , which is shown in (3) to produce the best clustering [45]. Euclidean distance has usually been employed to investigate the similarity metric [45]. Due to the structure of the data used in this study, the Euclidean distance is proposed to quantify and group the proximity of the data related to time. The Euclidean distance  $d_E$  is defined in (4).

$$J_m = \sum_{i=1}^k \sum_{x \in S_i} d(x, c(i))^2 \quad (3)$$

$$d_E(A, B) = \sum_{i=1}^N |a_i - b_i| \quad (4)$$

where  $d$  denotes the representative object of a particular centroid.  $c(i)$  is the particular cluster, and  $S$  is the total number of data points, whereas  $d_E$  is the Euclidean distance between  $A$  and  $B$  data points with  $N$  numeric attributes. The raw data clustering algorithm utilizing k-medoids is shown in Figure 4.

### 2.4. Methods

#### 2.4.1. Macor Sample

This research uses a Macor sample, which is a ceramic-based coating that mimics thermal barrier coatings (TBCs), as a flat representative sample. TBCs are used in aerospace and power generation industries, and this Macor sample with machined delamination is designed to resemble these coatings. The test sample is a perfect electric conductor (PEC) that has been insulated with non-porous (0% porosity) and low-loss glass ceramic (Macor) with a relative permittivity of 5.67 at 8.5 GHz.

The machined delamination's dimensions are  $20 \times 25$  mm,  $15 \times 15$  mm,  $10 \times 10$  mm, and  $5 \times 5$  mm. Aside from that, the delamination's depth ranges from 1 to 2 mm. Figure 5 illustrates the sample under test, along with the delamination's size and location, as well as the depth of the delamination between the PEC and the insulating layer. Table 3 lists the delamination size and depth for a manufactured Macor sample with machined delamination.

In order to demonstrate the delamination between the insulating layer and the metal substrate, the machining defect surface has been represented with by a metal sheet. The reverse surface of the Macor sample is then scanned with a Q-band OERW to determine the delamination size and location.

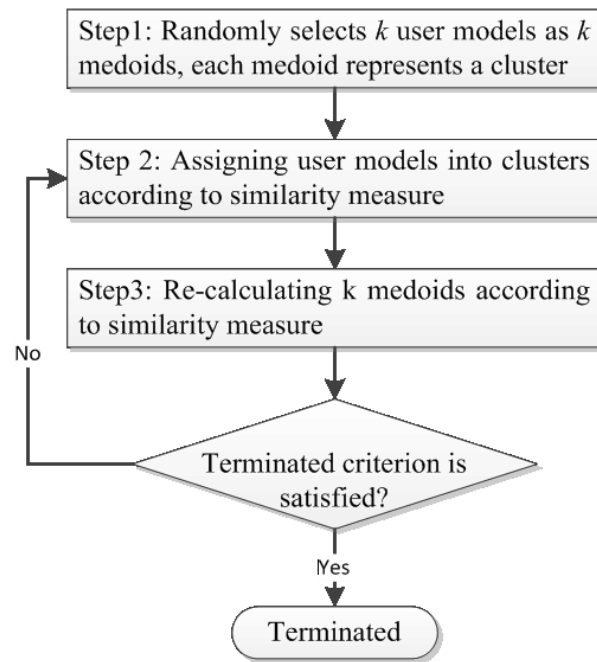


Figure 4. Raw data clustering of the k-medoids algorithm.

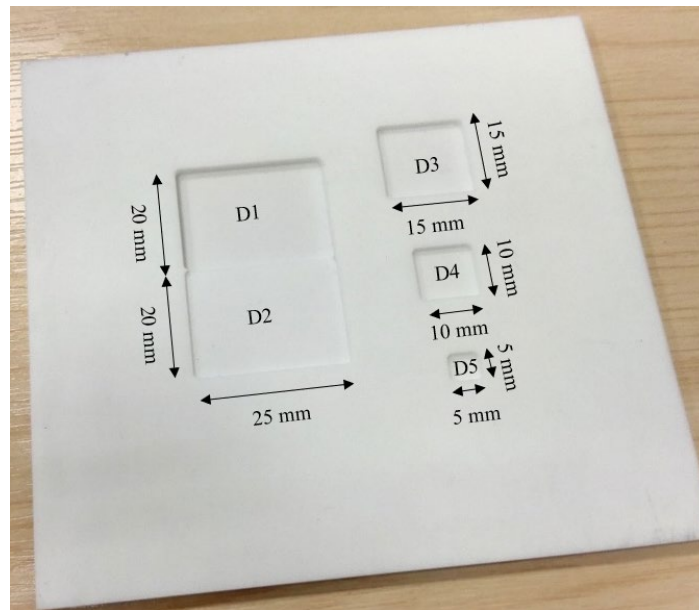


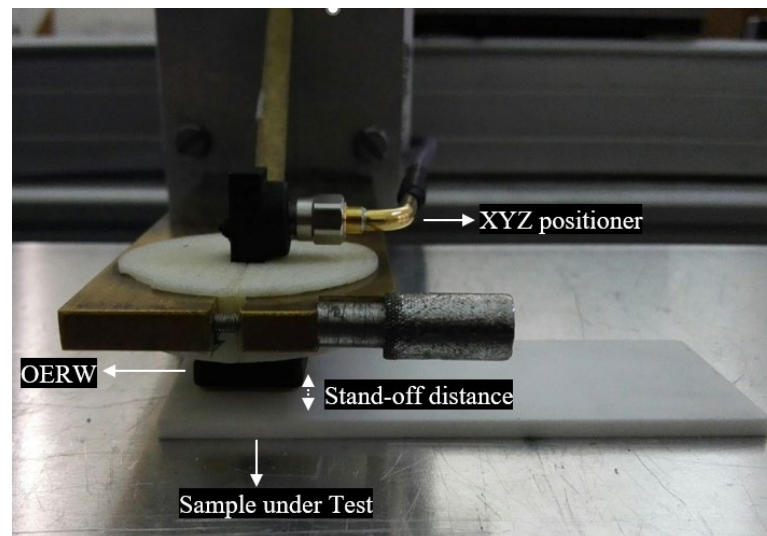
Figure 5. The sample under test with the delamination’s size and location.

Table 3. Actual delamination size and depth in fabricated Macor sample.

Macor Sample	Defect 1 (D1)	Defect 2 (D2)	Defect 3 (D3)	Defect 4 (D4)	Defect 5 (D5)
Delamination size	20 × 25 mm	20 × 25 mm	15 × 15 mm	10 × 10 mm	5 × 5 mm
Delamination depth	2 mm	1 mm	1.5 mm	1.5 mm	1.5 mm

#### 2.4.2. Inspection Technique

Figure 6 presents the configuration of the OERW inspection system.



**Figure 6.** Setup of the OERW inspection system.

The microwave sensor is a typical WR-22 OERW probe with a cross-sectional area of  $5.6 \times 2.8$  mm. The waveguide holder holds the OERW and performs raster scanning by using a step size of 1 mm in both the x- and y-directions. An XYZ positioner is used to execute the raster scanning. The XYZ positioner is configured to regulate the waveguide movement throughout the examination procedure. The scanning yields  $70 \times 70$  cells, which represent the x- and y-direction scanning points. The probe's standoff distance from the sample under test is adjusted to 1 mm. For the preparation of the VNA, it is subjected to an open-short-load (OSL) calibration process to remove the connector and cable errors. The measurement reference point is shifted to the cables' tip, which is the OERW waveguide's input port, during one port calibration. The OERW then operates in Q-band, which ranges from 33 to 50 GHz. Using a linear sweep with 101 frequency points at each examined site, the VNA is utilized to determine the complicated reflection coefficient acquired from the OERW waveguide. The Q-band OERW reflection coefficient data is in the form of the complex number and frequency domain. The examined location and frequency are saved in a matrix after the inspection. The complex reflection coefficient of the sample is saved in a 3D matrix  $S(m, n, f)$  as the last inspection outcome, where  $m$  and  $n$  indicate the position of the inspection, while  $f$  represents the operational frequency point from 1 to 101.

#### 2.4.3. Microwave Signal Processing

Despite the above, the OERW has several limitations in terms of characterizing the defect under the coating, such as blurred defect shape and low spectral resolution. Thus, signal processing approaches are necessary to precisely predict the defect's size and position. Figure 7 shows the work frame of the microwave NDT with the k-medoids clustering algorithm for defect detection and size estimation.

Each of the 101 frequency points at every single  $S(m, n)$  is transformed from the signals conveyed in terms of frequency to a time series, employing IFFT. After that, the complex time-domain data is also converted to the magnitude with the 'abs' function in Matlab (R2021a). This is because, in some cases of the time domain, the centroids' borders defined by the magnitude of the centroids in defect-free areas are greater than in the defect areas [15,18]. Therefore, it is easier to observe the defect and non-defect centroids.

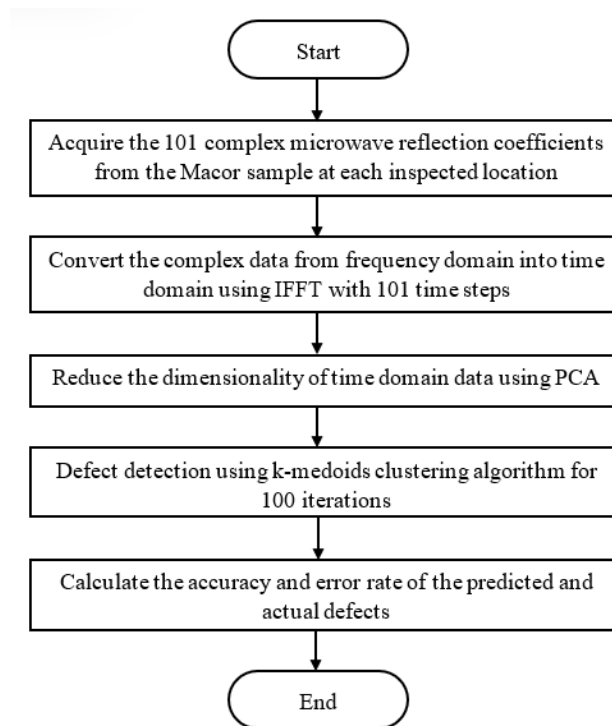


**Figure 7.** Work frame of microwave NDT with k-medoids clustering algorithm for defect detection and size estimation.

PCA was used to reduce the 101-time steps down to only three uncorrelated PCA components [46]. This dimensionality reduction for the features vector is required to speed up the processing time. Three of the PCA components can preserve the original data with maximum variances and perceive diverse characteristics to distinguish the defect and non-defect areas. The three PCA components are split into two known clusters—defect and non-defect clusters—employing the k-medoids clustering algorithm. The data points clustered in the defect group illustrate the location of the delamination in the Macor sample. Then, the k-medoids algorithm is set to run for 100 iterations. This is because the execution of k-medoids will obtain different clustering accuracy. By increasing the number of iterations, the maximum clustering accuracy can be acquired.

The data is compared to the size of the actual delamination defects after it has been clustered. The actual delamination defects are presented in the actual ground truth, as demonstrated in Figure 8.

The inspected areas for the coating in the ground truth, labeled 2 and 1, with regards to the actual defect and non-defect locations, respectively. The labeling depicts the Macor sample's actual defect shape, size, and location.

Actual and expected defect discrepancies are tabulated in terms of area, error rate, and accuracy. The accuracy percentage of the clustering results is calculated using (5), while the error rate of each predicted delamination's size is calculated as shown in (6).

$$Accuracy = \frac{TP + TN}{TP + TN + FP + FN} \quad (5)$$

$$Error\ rate\ (\%) = \frac{|D_p - D_A|}{D_A} \times 100\% \quad (6)$$

where  $TP$  is true positives,  $TN$  is true negatives,  $FP$  is false positive, and  $FN$  is false negative. Where  $D$  denotes as delamination sizes,  $p$  and  $A$  represent predicted and actual sizes, respectively.

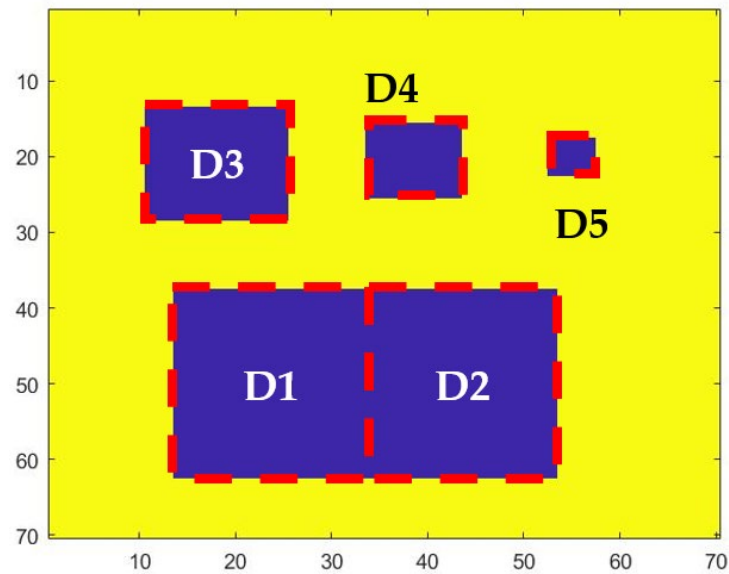


**Figure 8.** Ground truth labeling of accurate measurement, where D1, D2, D3, D4 and D5 denotes as Defect 1, Defect 2, Defect 3, Defect 4, and Defect 5, correspondingly.

### 3. Results

In the case of IFFT, the reflection coefficient obtained from the VNA is transformed from the signals conveyed in terms of frequency to a time series. After that, the k-medoids algorithm goes through a total of 100 maximum iterations before reaching a point where it settles on the best centroids as the final result. In this case, the number of cycles pertains to the centroids adjusted by the clusters' similar measurements. Upon reaching the last iteration, no shifts in centroids are observed. Accordingly, the k-medoid satisfies the halt criterion and produces reliable categorization outcomes. Figure 9 illustrates the optimal centroid of the reflection coefficient of the defect and defect-free areas in the time domain.

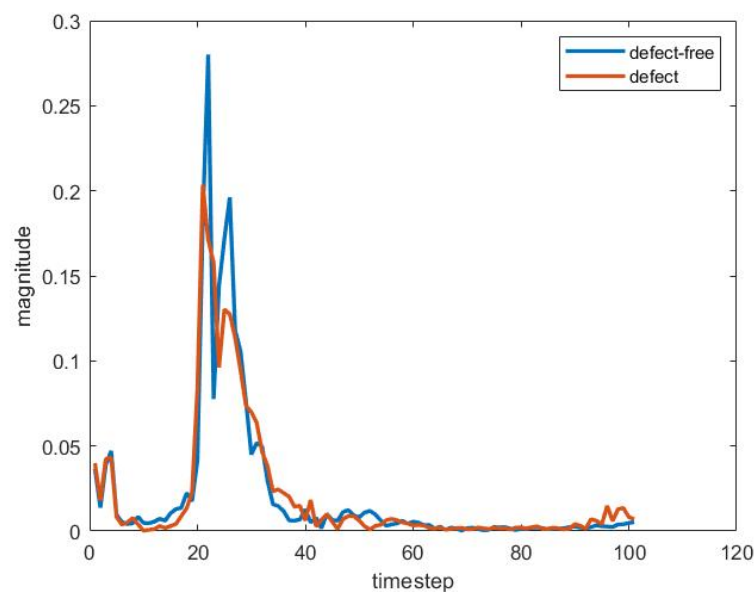


**Figure 9.** Centroid of reflection coefficient in the time domain after implementation of IFFT.

The proposed technique is capable of distinguishing the delamination and delamination-free signal. The amplitude of the flaws' signal is lower than the magnitude of the defect-free

signal. Figure 10 demonstrates the peaks of magnitude dispersion of delamination and delamination-free signals within the initial 45 time intervals.

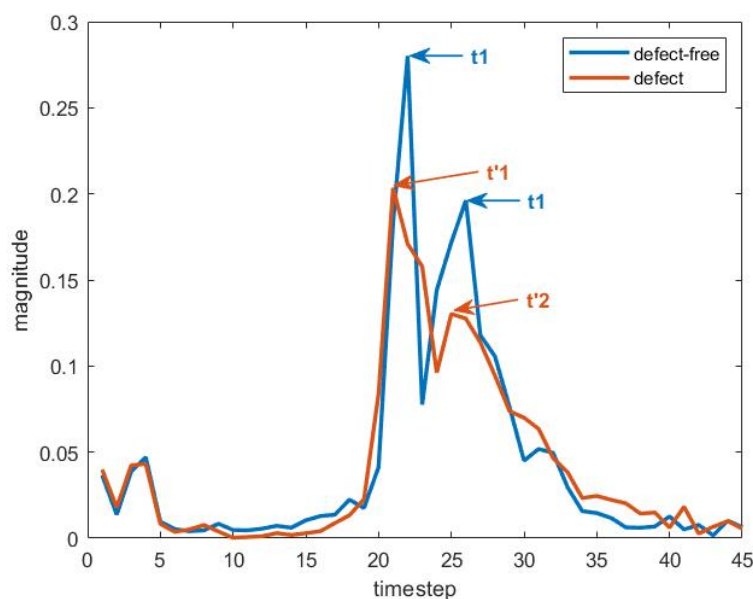


**Figure 10.** The peak of magnitude dispersion of delamination,  $t'_1$  and  $t'_2$  and delamination-free signals,  $t_1$  and  $t_2$  within the initial 45 time steps.

The magnitude of  $t_1$  and  $t_2$  of the defect-free zone is higher than the  $t'_1$  and  $t'_2$  magnitude of the defect zone. In this case, the reduction in the magnitude of the  $t_1$  and  $t_2$  can infer that delamination occurs in the ceramic coating. The defect and defect-free zones can be simply grouped by utilizing the magnitude of reflected microwave signals in the time domain using this deduction. Thus, the k-medoids clustering algorithm applies proximity to the centroids to split up the reflected microwave signals into delamination and delamination-free regions.

In the feature extraction stage, the dimensionality of 101 time steps is reduced into three PCA components using the PCA algorithm. The discrepancies between the defect and defect-free locations over the inspected sample are depicted by the variations in each PCA component. Figure 11 illustrates the three PCA components of the Macor sample, which are PC 1, PC 2, and PC 3, respectively.

The boundaries of the delamination are dispersed throughout all three PCA components. For example, the PC 2 can describe the boundaries of defects D2, D3, and D4. Meanwhile, the boundaries of all defects can be observed clearly in PC 1. In PC 3, only the boundaries of defects D3, D4, and D5 can be observed. The PCA preserves the dominant defect features for defect detection and sizing in all three PCA components. As a result, all three PCA components are sent into the k-medoids clustering algorithm to discriminate among the delamination and non-delamination locations in the Macor coating.

Figure 12 shows the scattering plot of each PCA component at the inspected location corresponding to the centroids of the defect and defect-free clusters using the k-medoids clustering algorithm.

It can be noted that the PCA components obtained from the defective locations are widely scattered due to the variations in defect depth and size. On the other hand, the PCA components of the defect-free locations are distributed closely, as the thickness of the Macor layer is constant (e.g., 3 mm). After all the data points have been grouped together, the cluster centroid of each group is then positioned in close proximity to the data points. According to the Euclidean distance as the determining factor, the data point is assigned to the centroid that is relatively nearest to it. The data point is considered as a defect-free zone if and only if it has a minimum Euclidean distance from the defect-free

centroid. In a the similar vein, the data point is deemed defective if the data point has a minimal Euclidean distance from the defect centroid. However, the PCA components of the defect-free locations are not completely overlapped due to surface roughness and porosity variations. To this end, the proposed k-medoids algorithm for microwave NDT has successfully measured the centroids of the defect and defect-free clusters that are capable of classifying each inspected location into defect or defect-free, based on the minimal Euclidean distance, with an acceptable degree of accuracy.

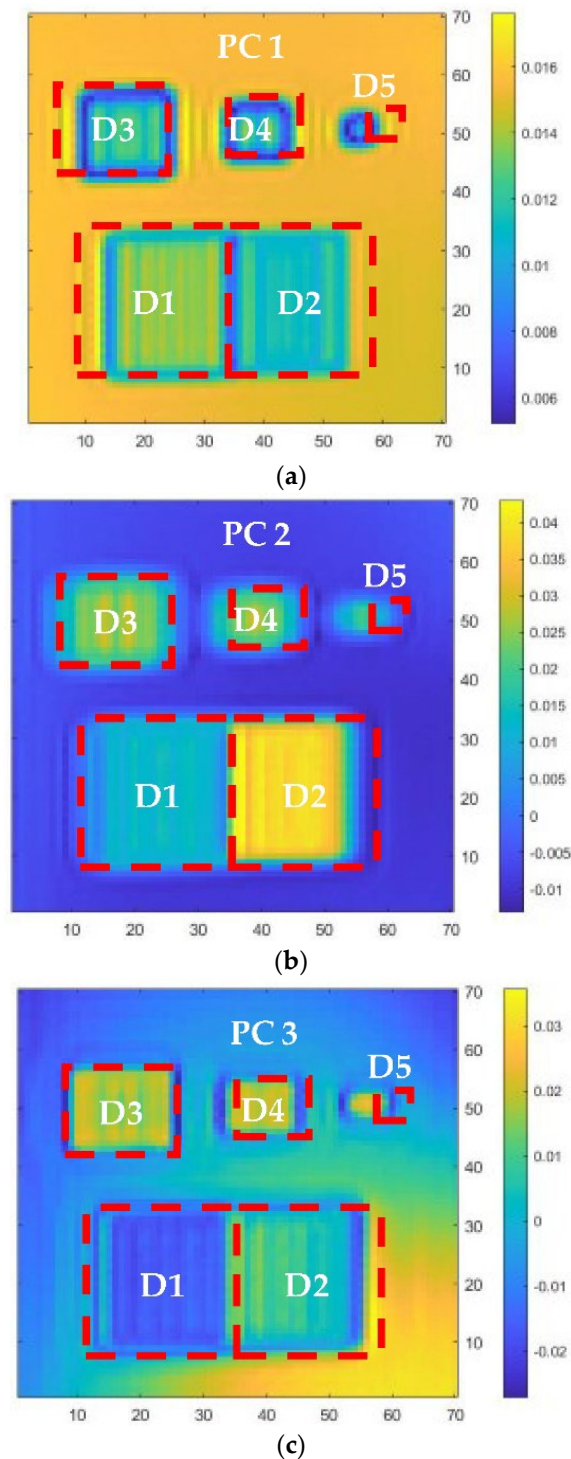


Figure 11. (a) PC 1, (b) PC 2, (c) PC 3 of the Macor sample.

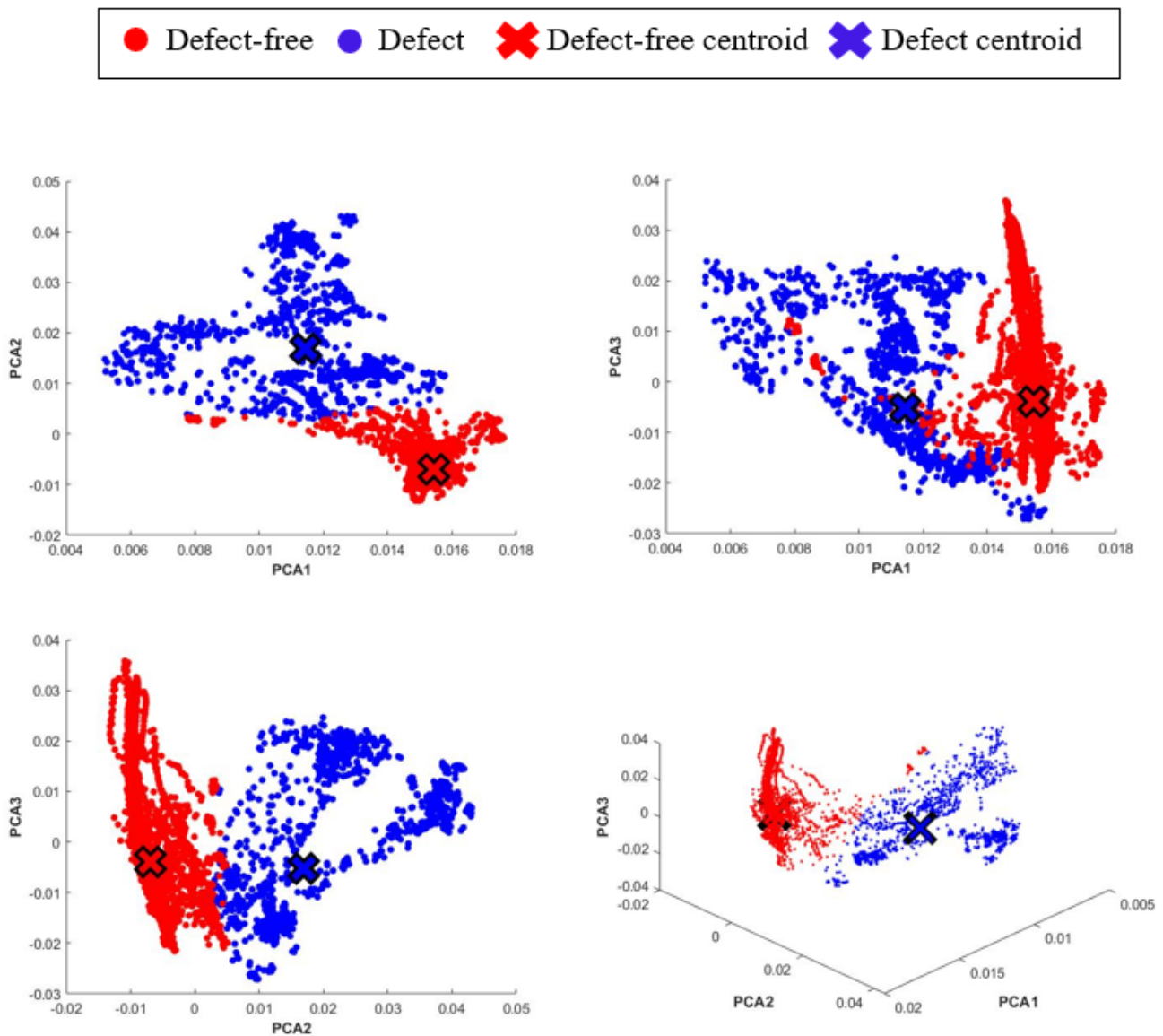


Figure 12. Scattering graphs depict the datasets from the three PCA components with regard to the groups of delamination and non-delamination for each investigated position.

Table 4 presents the margin of error of the defect size to evaluate the delamination size under the Macor sample.

Table 4. Clustering data of the k-medoids clustering algorithm.

Defects	Actual Defect Size (mm × mm)	Predicted Defect Size (mm <sup>2</sup> )	Actual Defect Area (mm × mm)	Predicted Defect Area (mm <sup>2</sup> )	Error Rate (%)	Accuracy (%)
D1	20 × 25	20 × 26	500	486	2.8	95.3878
D2	20 × 25	22 × 25	500	528	5.6	
D3	15 × 15	19 × 17	225	301	33.78	
D4	10 × 10	13 × 12	100	136	36	
D5	5 × 5	9 × 6	25	41	64	

All the five delamination defects are detected using the k-medoids clustering algorithm. The error rate of the predicted defect is calculated based on the area of the actual and predicted defect. The predicted defect size cannot be used as a precise representation

of the predicted defect, as there is some gaps in the anticipated defect size. The k-medoids algorithm achieve a maximum accuracy of 95.3878%. The predicted defects for  $20 \times 25$  mm achieved a less than 10% error rate. The error rate of D2 is higher than D1, as the delamination depth of D2 is lower than that of D1. This algorithm presents a higher accuracy in predicting larger delamination. In addition, the suggested approach is able to sharply separate the borders of the defects. Yet, the extent of delamination predicted is still larger compared to the real delamination size and area. Moreover, the prediction of smaller delamination is weak, as the error rate is too high.

In the case of k-medoids validation, a spatial image is used to evaluate the defect size in the Macor coating, as shown in Figure 13.

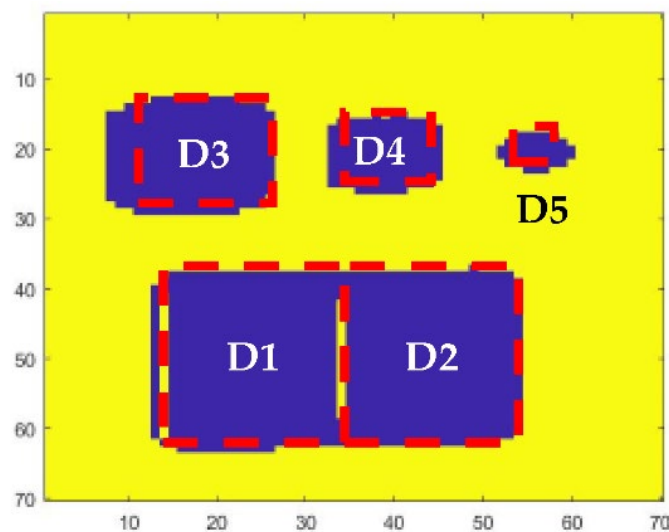


**Figure 13.** Spatial image using a k-medoids clustering algorithm.

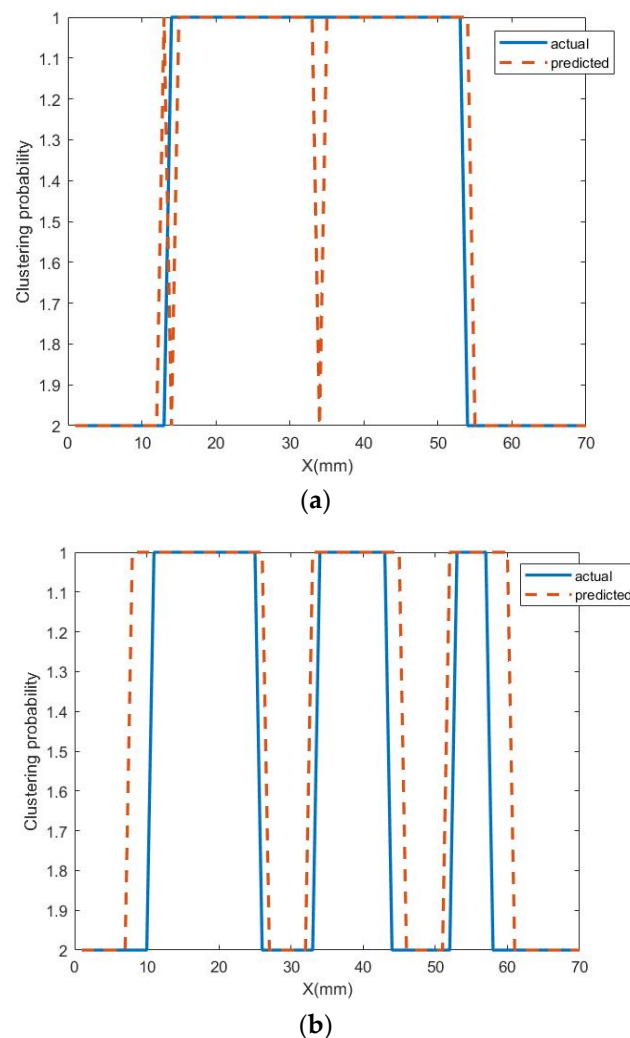
Spatial images are utilized to assess the delamination size in a Macor coating during the delamination size estimation stage in order to confirm the accuracy of the defect boundaries. The clustering algorithms assign each inspected location in the spatial images to 2 or 1 values, referring to defect or non-defect area, respectively. Every value on the spatial images corresponds to a 1 mm microwave probe scanning in the x- and y-direction. The spatial image is selected from the maximum accuracy rate among 100 runs of the k-medoids algorithm.

Figure 14 presents a juxtaposition among both the grouping outcomes to the real position and extent of the Macor sample.

Each delamination is dispersed according to its exact real position. The size of the defects predicted is slightly larger than the actual defects, despite the fact that the projected delamination location reveals a significant result.

This relatively higher estimation error for the smaller defects originates from the nature of the electromagnetic interaction between the waveguide's open end and the defected area. Generally, the interaction starts when the waveguide's edge reaches the beginning of the defect. Hence, the change in the reflection appears over an area larger than the defect by a factor that depends on the dimensions of the waveguide's aperture. In our case, this effect is not pronounced for D1, D2, and D3 due to their large area when compared to the WR-22 waveguide used in the measurements ( $5.6 \times 2.8$  mm). However, as the defect size approaches that of the aperture, as in D4 and D5, the enlargement effects become more pronounced, and the estimated defect size becomes larger.

Despite these slight estimation errors, the proposed technique provides a simple microwave NDT method for defect detection and sizing without intensive pre-knowledge that can be used in the industry as a part of a maintenance routine in real applications.



**Figure 14.** A juxtaposition among both the grouping outcomes to the real position and extent of the Macor sample (a)  $25 \times 20$  mm defects, (b)  $15 \times 15$  mm,  $10 \times 10$  mm, and  $5 \times 5$  mm defects.

#### 4. Conclusions

There has been a recent uptick of microwave NDT techniques in defect evaluation, both in the scientific communities and in industries. Despite their advantages, these methods still face some challenges before they can guarantee a high quality defect inspection, including overcoming issues such as standoff deviations and selecting the appropriate frequency points. The quality of defect evaluation can be improved by the use of soft computing algorithms, such as signal processing and artificial intelligence algorithms. Therefore, the constraints of defect inspection can be resolved, and a favorable outcome can be achieved via the combination of soft computing and microwave NDT techniques.

A novel microwave NDT using machine learning, which employed OERW based on k-medoids clustering algorithms to identify delaminations in the ceramic coating, was presented in this study. Currently, the defect assessment in regards to delamination position and extent utilizing the k-medoids clustering algorithm-based microwave NDT approach has not been disclosed elsewhere. Microwave reflection coefficients are used in conjunction with the suggested method to discover the underlying faults in the ceramic insulating layer. In order to reduce the impact of the permittivity changes on the reflected coefficients owing to the porosity of the ceramic coating, a tiny rectangular window is employed to measure the mean of the set of the neighboring points at each frequency point. The reflection coefficients are expressed in time domain form using IFFT. PCA is employed for feature extraction to reduce the dimensionality of the 3 PCA components. In the

last step, each inspected location is clustered into a defect or defect-free area using the k-medoids clustering algorithm, which identifies the delamination in the ceramic coating. The k-medoids approach demonstrates excellent clustering of defects, based on their real locations.

In this research, the k-medoids clustering algorithm shows a 95.3878% anticipated defect accuracy compared to the actual defects. The k-medoids algorithm presents a higher accuracy in predicting larger delaminations. Nonetheless, the regions of projected delamination are larger than the actual size of the defects. The suggested approach is capable of sharply distinguishing the borders of faults from the defect-free regions. Since the suggested approach requires fewer adaptations, it is more operationally friendly and may be utilized as an in situ microwave NDT system for defect detection. It can also be used as a portable field service inspection method and can be integrated into quality control processes in manufacturing.

**Author Contributions:** Conceptualization, S.Y.T. and N.H.M.M.S.; methodology, S.Y.T.; software, S.Y.T.; validation, S.Y.T., N.H.M.M.S. and M.F.A.; formal analysis, S.Y.T.; investigation, S.Y.T.; resources, S.Y.T. and M.F.A.; data curation, S.Y.T.; writing—original draft preparation, S.Y.T.; writing—review and editing, N.H.M.M.S., M.F.A., M.N.A.W. and G.N.J.; visualization, S.Y.T.; supervision, M.F.A.; project administration, S.Y.T. and M.F.A.; funding acquisition, M.F.A. and M.N.A.W. All authors have read and agreed to the published version of the manuscript.

**Funding:** This research was funded by the Ministry of Higher Education, Malaysia, Fundamental Research Grant Scheme Project FRGS/1/2020/STG06/USM/02/4.

**Institutional Review Board Statement:** Not applicable.

**Informed Consent Statement:** Not applicable.

**Data Availability Statement:** Not applicable.

**Conflicts of Interest:** The authors declare no conflict of interest.

## References

1. Zhao, Z. Review of Non-Destructive Testing Methods for Defect Detection of Ceramics. *Ceram. Int.* **2021**, *47*, 4389–4397. [[CrossRef](#)]
2. Akbar, M.F.; Jawad, G.N.; Duff, C.I.; Sloan, R. Porosity Evaluation of In-Service Thermal Barrier Coated Turbine Blades Using a Microwave Nondestructive Technique. *NDT E Int.* **2018**, *93*, 64–77. [[CrossRef](#)]
3. Akbar, M.F.; Jawad, G.N.; Danoon, L.R.; Sloan, R. Delamination Detection in Glass-Fibre Reinforced Polymer (GFRP) Using Microwave Time Domain Reflectometry. In Proceedings of the 15th European Radar Conference (EuRAD), Madrid, Spain, 26–28 September 2018; pp. 253–256. [[CrossRef](#)]
4. Yee, T.S.; Akbar, M.F.; Ghazali, N.A.; Mohamed, M.F.P. Defects Detection Using Complementary Split Ring Resonator with Microstrip Patch Antenna. In *Lecture Notes in Electrical Engineering, Proceedings of the 11th International Conference on Robotics, Vision, Signal Processing and Power Applications, Malaysia, 11 February 2022*; Mahyuddin, M.N., Norr, M.R.N., Sakim, M.A.H., Eds.; Springer: Berlin/Heidelberg, Germany, 2022; pp. 625–631. [[CrossRef](#)]
5. Akbar, M.F. Material Characterisation and Nondestructive Testing Using Microwave Technique. Ph.D. Thesis, University of Manchester, Manchester, UK, 2018.
6. Taheri, H.; Hassen, A.A. Nondestructive Ultrasonic Inspection of Composite Materials: A Comparative Advantage of Phased Array Ultrasonic. *Appl. Sci.* **2019**, *9*, 1628. [[CrossRef](#)]
7. Shi, L.; Long, Y.; Wang, Y.; Chen, X.; Zhao, Q. On-Line Detection of Porosity Change of High Temperature Blade Coating for Gas Turbine. *Infrared Phys. Technol.* **2020**, *110*, 103415. [[CrossRef](#)]
8. Akbar, M.F.; Sloan, R.; Duff, C.; Wielgat, M.; Knowles, J. Nondestructive Testing of Thermal Barrier Coated Turbine Blades Using Microwave Techniques. *Mater. Eval.* **2016**, *74*, 543–551.
9. Li, Z.; Wang, P.; Haigh, A.; Soutis, C.; Gibson, A. Review of Microwave Techniques Used in the Manufacture and Fault Detection of Aircraft Composites. *Aeronaut. J.* **2021**, *125*, 151–179. [[CrossRef](#)]
10. Viegas, C.; Alderman, B.; Huggard, P.G.; Powell, J.; Parow-Souchon, K.; Firdaus, M.; Liu, H.; Duff, C.I.; Sloan, R. Active Millimeter-Wave Radiometry for Nondestructive Testing/Evaluation of Composites-Glass Fiber Reinforced Polymer. *IEEE Trans. Microw. Theory Tech.* **2017**, *65*, 641–650. [[CrossRef](#)]
11. Teng, W.S.; Akbar, M.F.; Jawad, G.N.; Tan, S.Y.; Sazali, M.I.S.M. A Past, Present, and Prospective Review on Microwave Nondestructive Evaluation of Composite Coatings. *Coatings* **2021**, *11*, 913. [[CrossRef](#)]

12. Yee, T.S.; Akbar, M.F. Under Insulation Microwave Non-Destructive Testing Using Dual-Ridges Open-Ended Rectangular Waveguide. In *Lecture Notes in Electrical Engineering, Proceedings of the 11th International Conference on Robotics, Vision, Signal Processing and Power Applications, Malaysia, 11 February 2022*; Mahyuddin, M.N., Norr, M.R.N., Sakim, M.A.H., Eds.; Springer: Berlin/Heidelberg, Germany, 2022; pp. 684–689. [\[CrossRef\]](#)
13. Shrifan, N.H.M.M.; Akbar, M.F.; Isa, N.A.M. Prospect of Using Artificial Intelligence for Microwave Nondestructive Testing Technique: A Review. *IEEE Access* **2019**, *7*, 110628–110650. [\[CrossRef\]](#)
14. Shrifan, N.H.M.M.; Akbar, M.F.; Isa, N.A.M. An Adaptive Outlier Removal Aided K-Means Clustering Algorithm. *J. King Saud Univ. Comput. Inf. Sci.* **2021**, *34*, 1–12. [\[CrossRef\]](#)
15. Shrifan, N.H.M.M.; Jawad, G.N.; Isa, N.A.M.; Akbar, M.F. Microwave Nondestructive Testing for Defect Detection in Composites Based on K-Means Clustering Algorithm. *IEEE Access* **2021**, *9*, 4820–4828. [\[CrossRef\]](#)
16. Case, J.T.; Kenderian, S. Microwave NDT: An Inspection Method. *Mater. Eval.* **2017**, *75*, 339–346.
17. Rahman, M.S.U.; Yassin, A.; Abou-Khousa, M.A. Microwave Imaging of Thick Composite Structures Using Circular Aperture Probe. *Meas. Sci. Technol.* **2018**, *29*, 095403. [\[CrossRef\]](#)
18. Akbar, M.F.; Shrifan, N.H.M.M.; Jawad, G.N.; Isa, N.A.M. Assessment of Delamination Under Insulation Using Ridge Waveguide. *IEEE Access* **2022**, *10*, 36177–36187. [\[CrossRef\]](#)
19. Savin, A.; Novy, F.; Fintova, S.; Steigmann, R. Evaluation of Thin Discontinuities in Planar Conducting Materials Using the Diffraction of Electromagnetic Field. In *IOP Conference Series: Materials Science and Engineering, Proceedings of the ModTech International Conference-Modern Technologies in Industrial Engineering V, Sibiu, Romania 14–17 June 2017*; IOP Publishing Ltd.: Bristol, UK, 2017. [\[CrossRef\]](#)
20. Li, Z.; Haigh, A.; Soutis, C.; Gibson, A.; Sloan, R. A Simulation-Assisted Non-Destructive Approach for Permittivity Measurement Using an Open-Ended Microwave Waveguide. *J. Nondestruct. Eval.* **2018**, *37*, 1–10. [\[CrossRef\]](#)
21. Ghasr, M.T.; Horst, M.J.; Lechuga, M.; Rapoza, R.; Renoud, C.J.; Zoughi, R. Accurate One-Sided Microwave Thickness Evaluation of Lined-Fiberglass Composites. *IEEE Trans. Instrum. Meas.* **2015**, *64*, 2802–2812. [\[CrossRef\]](#)
22. Zoughi, R.; Gallion, J.R.; Ghasr, M.T. Accurate Microwave Measurement of Coating Thickness on Carbon Composite Substrates. *IEEE Trans. Instrum. Meas.* **2016**, *65*, 951–953. [\[CrossRef\]](#)
23. Akbar, M.F.; Jawad, G.N.; Rashid, L.D.; Sloan, R. Nondestructive Evaluation of Coatings Delamination Using Microwave Time Domain Reflectometry Technique. *IEEE Access* **2020**, *8*, 114833–114841. [\[CrossRef\]](#)
24. Akbar, M.F.; Sloan, R.; Duff, C.I.; Wielgat, M.; Knowles, J.F. Microwave Nondestructive Evaluation of Thermal Barrier Coated Turbine Blades Using Correlation Analysis. In *Proceedings of the 46th European Microwave Week 2016: “Microwaves Everywhere”, European Microwave Conference, EuMC 2016, London, UK, 3–7 October 2016*; pp. 520–523. [\[CrossRef\]](#)
25. Shrifan, N.H.M.M.; Akbar, M.F.; Isa, N.A.M. Maximal Overlap Discrete Wavelet-Packet Transform Aided Microwave Nondestructive Testing. *NDT E Int.* **2021**, *119*, 102414. [\[CrossRef\]](#)
26. Edis, E.; Flores-Colen, I.; de Brito, J. Time-Dependent Passive Building Thermography for Detecting Delamination of Adhered Ceramic Cladding. *J. Nondestruct. Eval.* **2015**, *34*, 1–16. [\[CrossRef\]](#)
27. Qin, B.; Hu, C.; Huang, S. Target/Background Classification Regularized Nonnegative Matrix Factorization for Fluorescence Unmixing. *IEEE Trans. Instrum. Meas.* **2016**, *65*, 874–889. [\[CrossRef\]](#)
28. Sanchez-Suarez, R.M.; Choquehuanca-Zevallos, J.J.; Huamán-Mamani, F.A.; Mayta-Ponce, D.L.; Ludeña-Choez, J. A Method Based on RF Spectral Features for Evaluating the Porosity Degree in Ceramic Materials. In *Proceedings of the 2018 IEEE MTT-S Latin America Microwave Conference, LAMC, Arequipa, Peru, 12–14 December 2018*. [\[CrossRef\]](#)
29. Kraljevski, I.; Duckhorn, F.; Tschope, C.; Wolff, M. Machine Learning for Anomaly Assessment in Sensor Networks for NDT in Aerospace. *IEEE Sens. J.* **2021**, *21*, 11000–11008. [\[CrossRef\]](#)
30. Agarwal, S.; Singh, D. Optimal Non-Invasive Fault Classification Model for Packaged Ceramic Tile Quality Monitoring Using MMW Imaging. *J. Infrared Millim. Terahertz Waves* **2016**, *37*, 394–413. [\[CrossRef\]](#)
31. James, R.; Kim, T.H.; Narayanan, R.M. Prognostic Investigation of Galvanic Corrosion Precursors in Aircraft Structures and Their Detection Strategy. In *SPIE Conference on Nondestructive Characterization and Monitoring of Advanced Materials, Aerospace, and Civil Infrastructure, and Transportation XI, Portland, Oregon, USA, 26–29 March 2017*; Shull, J.P., Gyekenyesi, L.A., Wu, F.H., Eds.; SPIE: Bellingham, WA, USA, 2017; pp. 91–102. [\[CrossRef\]](#)
32. Martinez, J.A.; Belenguer, A.; Esteban, H. Fast Frequency Sweep Technique Based on Segmentation for the Acceleration of the Electromagnetic Analysis of Microwave Devices. *Appl. Sci.* **2019**, *9*, 1118. [\[CrossRef\]](#)
33. Jawad, G.N.; Akbar, M.F. IFFT-Based Microwave Non-Destructive Testing for Delamination Detection and Thickness Estimation. *IEEE Access* **2021**, *9*, 98561–98572. [\[CrossRef\]](#)
34. Alkandari, A.; Aljaber, S.J. Principle Component Analysis Algorithm (PCA) for Image Recognition. In *Proceedings of the 2015 2nd International Conference on Computing Technology and Information Management, ICCTIM, Johor, Malaysia, 21–23 April 2015*; pp. 76–80. [\[CrossRef\]](#)
35. Yin, Y.; Liu, F.; Zhou, X.; Li, Q. An Efficient Data Compression Model Based on Spatial Clustering and Principal Component Analysis in Wireless Sensor Networks. *Sensors* **2015**, *15*, 19443–19465. [\[CrossRef\]](#)
36. Ba, A.; Bui, H.-K.; Berthiau, G.; Yi, Q.; Zhu, J.; Tian, G.Y. Eddy-Current Pulsed Thermography for the Detection of Impact Damage on CFRP. In *Proceedings of the 11th International Symposium on NDT in Aerospace, Paris-Saclay, France, 13–15 November 2019*.

37. Adiwijaya, K.; Wisesty, U.N.; Aditsania, A.; Kusumo, D. Dimensionality Reduction Using Principal Component Analysis for Cancer Detection Based on Microarray Data Classification Analysis of Watermaking Using SVD Based on DWT and DCT View Project. *Artic. J. Comput. Sci.* **2018**, *14*, 1521–1530. [[CrossRef](#)]
38. Sun, Y.; Tao, X.; Li, Y.; Lu, J. Robust 2D Principal Component Analysis: A Structured Sparsity Regularized Approach. *IEEE Trans. Image Process.* **2015**, *24*, 2515–2526. [[CrossRef](#)]
39. Xu, C.; Zhou, N.; Xie, J.; Gong, X.; Chen, G.; Song, G. Investigation on Eddy Current Pulsed Thermography to Detect Hidden Cracks on Corroded Metal Surface. *NDT E Int.* **2016**, *84*, 27–35. [[CrossRef](#)]
40. Reddy, G.T.; Reddy, M.P.K.; Lakshmana, K.; Kaluri, R.; Rajput, D.S.; Srivastava, G.; Baker, T. Analysis of Dimensionality Reduction Techniques on Big Data. *IEEE Access* **2020**, *8*, 54776–54788. [[CrossRef](#)]
41. Allegretta, I.; Marangoni, B.; Manzari, P.; Porfido, C.; Terzano, R.; de Pascale, O.; Senesi, G.S. Macro-Classification of Meteorites by Portable Energy Dispersive X-Ray Fluorescence Spectroscopy (PED-XRF), Principal Component Analysis (PCA) and Machine Learning Algorithms. *Talanta* **2020**, *212*, 120785. [[CrossRef](#)] [[PubMed](#)]
42. MacHidon, A.L.; MacHidon, O.M.; Ogrutan, P.L. Face Recognition Using Eigenfaces, Geometrical PCA Approximation and Neural Networks. In Proceedings of the 2019 42nd International Conference on Telecommunications and Signal Processing, TSP 2019, Budapest, Hungary, 1–3 July 2019; pp. 80–83. [[CrossRef](#)]
43. Onan, A. A K-Medoids Based Clustering Scheme with an Application to Document Clustering. In Proceedings of the 2nd International Conference on Computer Science and Engineering, UBKM, Antalya, Turkey, 5–8 October 2017; pp. 354–359. [[CrossRef](#)]
44. Yu, D.; Liu, G.; Guo, M.; Liu, X. An Improved K-Medoids Algorithm Based on Step Increasing and Optimizing Medoids. *Expert Syst. Appl.* **2018**, *92*, 464–473. [[CrossRef](#)]
45. Martino, A.; Rizzi, A.; Massimo, F.; Mascioli, F. Efficient Approaches for Solving the Large-Scale k-Medoids Problem. In Proceedings of the 9th International Joint Conference on Computational Intelligence, International Joint Conference on Computational Intelligence, Funchal-Madeira, Portugal, 1–3 November 2017; Springer: Berlin/Heidelberg, Germany, 2017. [[CrossRef](#)]
46. Zhang, H.; Xu, L.; Wu, R.; Simm, A. Sweep Frequency Microwave NDT for Subsurface Defect Detection in GFRP. *nsight Non-Destr. Test. Cond. Monit.* **2018**, *65*, 123–129. [[CrossRef](#)]